The Interplay of Nanoconfinement and pH from the Perspective of a Dye-Reporter Molecule

Robert Brilmayer+,[a] Martin Brodrecht+,[b] Christoph Kaiser,[c] Hergen Breitzke,[b] Bharti Kumari,[b] Josef Wachtveitl,[c] Gerd Buntkowsky,*[b] and Annette Andrieu-Brunsen*[a]

Abstract: A novel thiazol-based ratiometric dye for the detection of local pH values is synthesized, and its properties are characterized by a combination of optical spectroscopy, solid-state NMR and DNP (dynamic nuclear polarization)-enhanced solid-state NMR. This novel dye covers a completely different sensitivity range with its acidic pKa value of 3.5 compared to other established dyes for ratiometric pH detection, such as SNARF. The dye is grafted to the surfaces of mesoporous silica materials, which enables, for the first time, direct in situ measurements of the local pH values in silica mesopores by a simple UV-vis spectroscopy method. The obtained results, which are in good agreement with previous indirect techniques, indicate a background electrolyte-dependent pKa shift of at least one pH unit under nanoconfined conditions compared to the pKa of the dye in bulk solution.

Introduction

Since their discovery in 1992, template-based mesoporous silica materials (MSMs) have attracted increasing interest in various research fields.[1] Currently, MSMs are commonly used in applications such as sensing,[2] separation processes[3] and energy conversion.[4] MSMs have interesting properties, such as a high specific surface area, high chemical stability and high physical stability.[5] In addition to these attributes, the surface silanol groups can be used to introduce organic functional groups in the inorganic framework.[5–6] This has been particularly relevant for mesoporous silica thin films as well as for mesoporous silica nanoparticles.[7] Functionalization with responsive organic moieties has led to the formation of smart materials in this research field, which has been of significant relevance in the past 15 years.[6,8] In these smart or responsive materials as well as in the application areas of smart materials such as drug delivery or environmental sensing, pH plays a crucial role; thus, and its influence has been studied extensively.

For example, enzyme stabilization is pH-dependent.[9] For drug delivery often minimal pH-changes in the exterior of mesoporous particles should induce a release.[10]

In this context, differences between the pH value in solution and under nanoconfined conditions, for example, within silica mesopores, have been reported based on theoretical studies and indirect experimental observations.[11] To date, experimental studies have been limited to indirect measurements such as ion flow through nanochannels or mesopore permselectivity to determine the charge of molecules inside nanoscale environments.[7,9a,12] Although pH detection in MSMs has gained more importance in recent years, the direct measurement of the apparent pH value inside nanopores has not yet been fully explored.[11b,13] The most prominent recent advances can be ascribed to theoretical studies by *Szleifer* and co-workers, who demonstrated the pKa shift of polyelectrolytes in nanochannels.[11a] Until now, the experimental determination and prediction of pH values in nanopores or nanochannels has remained a challenge but represents a crucial confinement parameter to understand in detail the transport, release, and molecular stabilization processes of mesoporous materials.[8b] One promising approach to investigate the pH value at the nanoscale has been the use of dyes.

In the context of dyes as pH reporter molecules, the main focus over the last few years has been to detect pH changes in cells. In this research field, various studies have explored pH changes in cancer cells compared to healthy cells, offering a new cancer detection method.[14] Due to the nature of living cells, those studies focused on a very narrow pH detection range (pH 6.5–7.6). However, to cover the entire relevant range of functionalized nanopores and their applications, dyes with sensitivity ranges between pH 1 and 5 are also needed. Potential dye sensors that have been explored together with mesoporous silica materials are FRET (*Förster resonance energy transfer*) dye pairs consisting of a pH-sensitive reporter and a pH-insensitive dye for concentration calibration. Due to the distinct nature of FRET, a constant distance between the donor

[a] Dr. R. Brilmayer,+ Prof. Dr. A. Andrieu-Brunsen
Ernst-Berl-Institut für Technische und Makromolekulare Chemie
Technische Universität Darmstadt
Alarich-Weiss-Str. 12, 64287 Darmstadt (Germany)
E-mail: andrieu-brunsen@smartmem.tu-darmstadt.de

[b] Dr. M. Brodrecht,+ Dr. H. Breitzke, Dr. B. Kumari, Prof. Dr. G. Buntkowsky
Eduard-Zintl-Institut für Anorganische und Physikalische Chemie
Technische Universität Darmstadt
Alarich-Weiss-Str. 8, 64287 Darmstadt (Germany)
E-mail: gerd.buntkowsky@chemie.tu-darmstadt.de

[c] C. Kaiser, Prof. Dr. J. Wachtveitl
Institute for Physical and Theoretical Chemistry, Goethe University
Max-von-Laue-Str. 7, 60438 Frankfurt (Germany)

[+] Both authors contributed equally.

and the acceptor molecule has to be retained to allow reproducible FRET with this pH detection method. Since this is a parameter that cannot be easily controlled in bulk solution and cannot be precisely characterized on surfaces or in mesopores, the use of FRET-dye pairs is not suitable for comparisons between measurements in nanoconfined conditions and in bulk solution.[11b] Ratiometric dyes, which have a distinct absorption and/or emission maximum in their protonated and deprotonated states, can overcome the issues of FRET pH reporters for use in nanopores. Additionally, the spectral maxima of ratiometric dyes are concentration independent, which further facilitates comparisons between different measurements.[13] Of the ratiometric dyes, many commonly applied in-cell dyes, such as the SNARF (Seminaphtharhodafluor) dye family, have a sensitivity region that does not overlap with the pKa value of silanol groups in mesoporous silica. One dye family that meets all the requirements mentioned above is the thiazol-based family of dyes such as the 5-methoxy-pyridylthialzole (MPT) dye reported by *Zheng et al.*[13b] These dyes are of special interest in combination with silica materials since their pKa value is in the responsive range of silanol groups.[12c,d,13b,15] Several similar dyes have been reported even recently as pH-reporters[16] for sensing vapor chromism in halogenated solvents[17] or ion sensors[18] usually applied while being dissolved but not covalently grafted to a surface.

To address the pH region between 1.5 and 5.0 in nanoscale pores in this study, we synthesized and investigated the potential of a new MPT-based ratiometric pH reporter dye in conjunction with MSMs. In addition to the characterization and determination of the optical properties, the successful attachment of the dye to the silica framework was confirmed by solid-state NMR, TGA (thermogravimetric analysis), EA (elemental analysis) and BET (Brunauer-Emmett-Teller)-based nitrogen adsorption-desorption measurements. Last, MPT−Ph was successfully used to determine pH shifts between bulk solutions and silica mesopores with diameters smaller than 20 nm. Therefore, pH shifts of more than one pH unit were observed.

Results and Discussion

Synthesis and optical properties of MPT−Ph

MPT−Ph (4-(5-methoxy-2-(pyridin-4-yl)thiazol-4-yl)benzoic acid) **2** and MPT-amide (4-(5-methoxy-2-(pyridin-4-yl)thiazol-4-yl)-N-propylbenzamide) **3** were synthesized as outlined in Scheme 1a.

MPT−Br (4-bromo-5-methoxy-2-(pyridin-4-yl)thiazole) **1** was synthesized in three steps according to a method established for MPT-based dyes by *Zheng et al.*[13b,15a] C−C bond formation was achieved by a *Suzuki* coupling reaction to form MPT−Ph **2**, followed by amination to yield MPT−Ph-amide **3**. Compounds **2** and **3** were characterized by 1D- and 2D-NMR as well as SI-MS (Figures S1−S8).

MPT compound **1** is an acidochromic chromophore since its absorbance and emission show a bathochromic shift upon acidification which probably results in protonation on the pyridine moiety.[13b] The effects of the introduction of the

phenyl group (MPT−Ph **2**) on the photophysical properties of MPT−Br **1** are depicted in Figure 1b. For the protonated (Figure 1b, green) and deprotonated MPT−Ph species (Figure 1b, blue), the absorption and fluorescence peaks show a bathochromic shift by approximately 50 nm compared to those of MPT−Br **1**. This is ascribed to the significant enlargement of the electronic π-system of MPT−Ph **2**. Regarding MPT−Ph, protonation of the N-basic site results in a redshift of the emission band from approximately 450 nm to 510 nm. The introduction of the positive charge results in a more pronounced charge displacement and a reduced transition energy for MPT−Ph (Figure 1c).

The molar extinction coefficients of both MPT−Ph and MPT−Ph-H$^+$ forms were determined by measurement of the concentration-dependent absorbance values at the maxima of their S1 bands. Following Lambert-Beer's law, the protonated and deprotonated forms exhibit extinction coefficients of 8070 ± 60 and 7440 ± 30 M^{-1} cm^{-1}, respectively (Figure S9). With the use of an integrating sphere, fluorescence quantum yields of 7% for the deprotonated form and 23% for the protonated form were calculated. The maximum emission signal can be obtained through excitation at the maxima of the S1 absorption bands for both species (Figure S10, 3D contour plots). The excitation spectrum, which is a vertical cut through the contour plots at the maximum emission wavelength, resembles the absorption spectrum. In the excitation wavelength-dependent contour plots, only the emission signals of the particular species are observed. Upon excitation of the deprotonated species at pH 7.4, no emission of the protonated form is detected, which indicates that the pyridine group does not act as a strong photobase and acquires a proton from the solvent, similar to related nitrogen-containing compounds reported in the literature.[19] Interestingly, the fluorescence decays of MPT−Ph, recorded by means of the time-correlated single photon counting (TCSPC) method, are significantly accelerated compared to other MPT derivatives.[13b] The decay curve of the protonated form MPT−Ph-H$^+$ could be fitted monoexponentially, which revealed a lifetime of 1.4 ns (Figure 1d). For the deprotonated MPT−Ph, a sum of two exponential functions was required, where a 1.7% contribution of the 1.4 ns lifetime could be assigned to residual amounts of the protonated species at pH 7.4. The major contribution of 98.3% of a 0.3 ns lifetime accounts for the deprotonated form.

MPT−Ph as a pH reporter in silica mesopores

Two different mesoporous silica materials with comparable porous structures were used as frameworks to incorporate the MPT−Ph dye. Mesoporous silica thin films with pore diameters of 8 and 16 nm and film thicknesses of 200–1000 nm were prepared using sol-gel chemistry and evaporation-induced self-assembly as previously reported.[9a,20] Additionally, amino-functionalized mesoporous silica SBA-15 (Santa Barbara amorphous 15) particles were prepared by a previously reported strategy.[21] The amino groups were introduced by a cocondensation approach using tetraethyl orthosilicate (TEOS) and (3-amino-

a)

b)
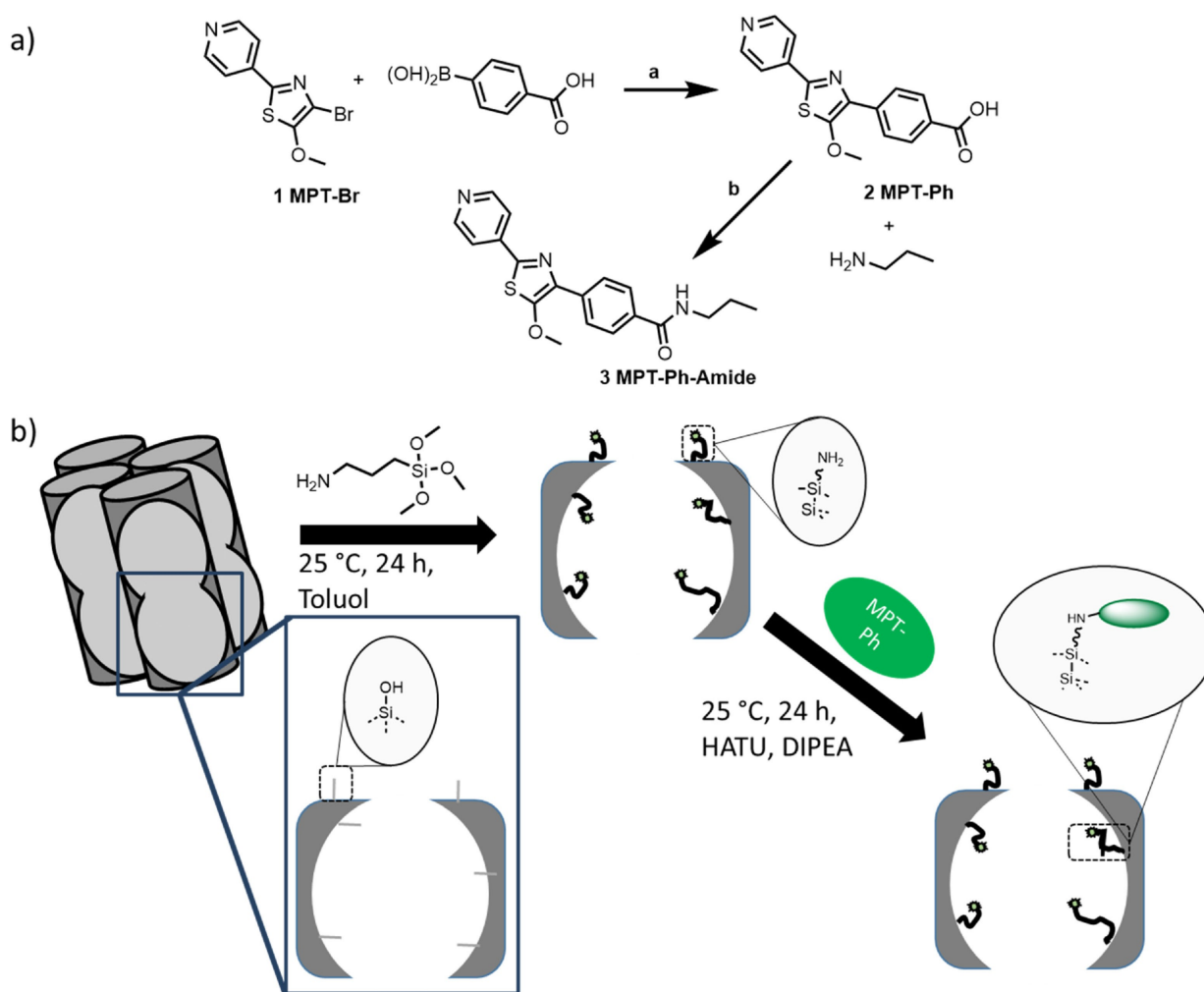
Scheme 1. (a) Synthesis of MPT–Ph (4-(5-methoxy-2-(pyridin-4-yl)thiazol-4-yl)benzoic acid) **2** and MPT-amide (4-(5-methoxy-2-(pyridin-4-yl)thiazol-4-yl)-N-propylbenzamide) **3**: a) X-Phos Pd G2 (chloro(2-dicyclohexylphosphino-2′,4′,6′-triisopropyl-1,1′-biphenyl)[2-(2′-amino-1,1′-biphenyl)]palladium(II)), dioxan/H_2O, K_2CO_3, reflux for 24 h under an inert atmosphere, 70%; b) HATU (O–N, N, N′, N′-tetramethyluronium-hexafluorphosphate), DIPEA (diisopropylethylamine), and DMF (N, N-dimethylformamide) reacted for 48 h under an inert atmosphere, 71%; (b) schematic illustration of silica modification. In the first step, aminopropyl trimethoxy silane (APTMS) is attached to the unfunctionalized silica pores. In a second step, MPT–Ph is coupled to the amino functional group through amide bond formation.

propyl)triethoxysilane (APTES). BET characterization of the SBA-15 materials is presented in detail in the supporting information (Figure S11–S14 and Table S1–S4).

To explore the influence of spatial confinement on the pH value inside of silica mesopores, the MPT–Ph pH reporter must be introduced into the silica framework while being accessible for the measurement solution, as illustrated for a postgrafting approach in Scheme 1b. For this purpose, covalent attachment of the dye is necessary to avoid leaching, which would result in a possible mixture of the dye in the mesopores and in the bulk solution.

The MPT–Ph dye carries a free carboxyl group that is not involved in pH detection and can thus be used as an anchor group. Amino groups are suitable reaction moieties resulting in amide bond formation under very mild reaction conditions. For this reason, the prepared mesoporous silica thin films were first functionalized with APTMS (aminopropyl trimethoxy silane) via

a postgrafting approach, while the amino functional groups in the SBA-15 material were introduced through cocondensation. In both cases, dye attachment through amide formation was performed using HATU (1-[Bis(dimethylamino)methylene]-1H-1,2,3-triazolo[4,5-b]pyridinium 3-oxide hexafluorophosphate) as the coupling reagent under identical reaction conditions.

Comparing TGA (thermogravimetric analysis) of the SBA-15 material before and after dye coupling (Figure S11), the weight fraction of the dye can be obtained (Table S1), leading to a dye loading of 0.33 ± 0.02 mmol/g. By applying elemental analysis (EA), the weight and molar fractions of the elements nitrogen, carbon and hydrogen are obtained (Table S2 and Table S3). Based on the result for nitrogen, a dye loading of 0.54 ± 0.05 mmol/g is calculated. The same process applies for carbon, leading to a dye loading of 0.55 ± 0.02 mmol/g.

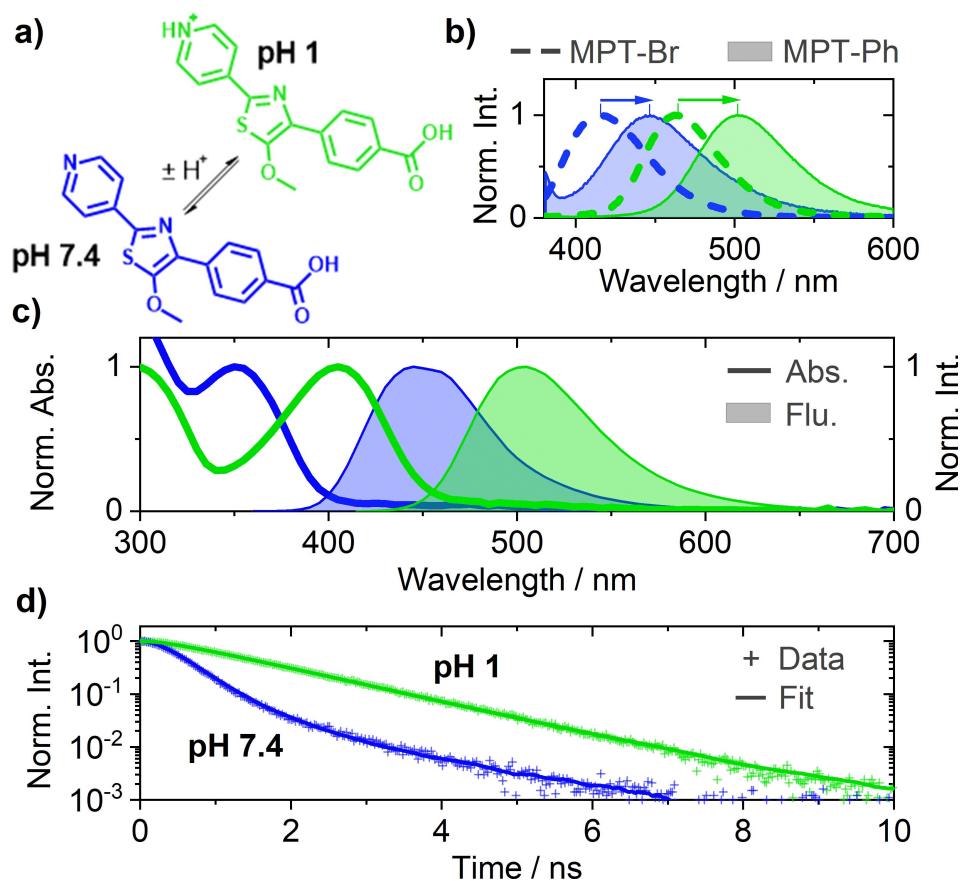The pore volume and specific surface area (Table S4) of the functionalized SBA-15 materials can be obtained by the

These are not the final page numbers! ↗↗

Figure 1. The protonated form of the MPT–Ph **2** dye and its spectrum at pH 1 is shown in green, and that of the deprotonated form at pH 7.4 is shown in blue. (a) Protonation reaction of MPT–Ph. (b) Emission spectra of the deprotonated and protonated forms of MPT–Br (dashed lines) and redshifted spectra of MPT–Ph (solid lines/green area). (c) Absorbance (solid lines) and emission spectra (filled areas) of MPT–Ph. (d) Fluorescence decays (+ symbols) and exponential fits (solid lines) of both forms of the MPT–Ph dye.

Brunauer-Emmett-Teller (BET) analysis of the nitrogen adsorption-desorption isotherms (Figure S12). To investigate changes in the pore diameter due to dye functionalization, Barrett-Joyner-Halenda (BJH) (Figure S13) and density functional theory (NLDFT) (Figure S14) methods are applied. While BJH analysis suggests a decrease in pore diameter from 5.6 ± 0.2 nm to 4.9 ± 0.3 nm, NLDFT analysis shows a decrease from 7.9 ± 0.2 nm to 6.6 ± 0.3 nm.

Combining the specific surface area of the dye-functionalized SBA-15 material (271 ± 7 m^2/g) and the results of the molar dye grafting densities by TGA and EA analysis, surface grafting densities of the dye can be calculated, and the results are shown in Table 1.

Both methods suggest a high degree of surface functionalization of the functionalized SBA-15 material. To investigate the

coupling efficiency and to prove the covalent binding of the MPT–Ph dye, NMR techniques were used. Since solid-state NMR requires a large amount of sample and a high degree of functionalization, these investigations were carried out with functionalized SBA-15 nanoparticles.

To monitor the success of the MPT–Ph dye modification, ^{13}C CP MAS solid-state NMR spectra were recorded before (Figure 2a) and after dye coupling (Figure 2c). A spectrum of the MPT–Ph dye was also included to facilitate the peak assignment (Figure 2b).

In the ^{13}C CP MAS spectrum of the APTES functionalized SBA-15 (Figure 2a), the signals at 9 ppm, 21 ppm and 43 ppm are assigned to the α, β and γ carbon atoms of the APTES ((3-aminopropyl)triethoxysilane)-linker, respectively. The small additional features at 18 ppm and 59 ppm are assigned to the not fully hydrolyzed ethoxy groups of either APTES or TEOS (tetraethoxysilane).

The spectrum of the pure MPT–Ph dye (Figure 2b) shows a signal at 66 ppm, which is characteristic of the carbon atom for the methoxy group (Me). The resonances between 127 ppm and 144 ppm can be assigned to the aromatic carbon atoms of the phenyl (Ph) and pyridine (Py) rings. Additionally, the peaks at 117 ppm, 161 ppm and 168 ppm can be assigned to the

Table 1. Calculated surface grafting densities of the MPT–Ph dye-functionalized SBA-15 material obtained by the combination of the specific surface area obtained by nitrogen adsorption-desorption and molar dye grafting densities obtained by TGA and EA.

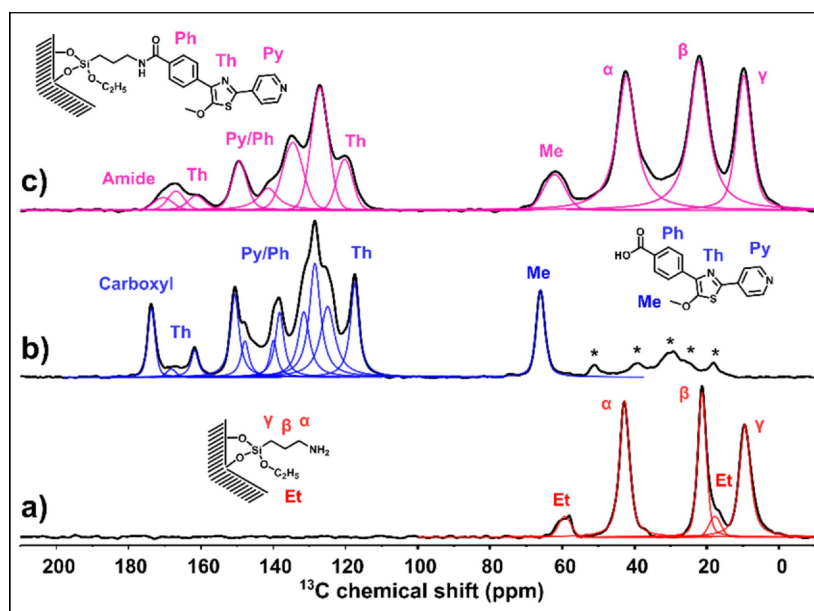|	TGA	EA (nitrogen)	EA (carbon)
Surface grafting density	0.73 ± 0.06	1.20 ± 0.14	1.22 ± 0.08

These are not the final page numbers! ↗↗

Figure 2. Comparison of the ^{13}C CP MAS spectra of the functionalized SBA-15 at a spinning rate of 6 kHz (10 kHz for (b) and (c)). From the bottom to the top spectra of the APTES functionalized SBA-15 (a), pure MPT–Ph dye (b) and MPT–Ph dye-functionalized SBA-15 species (c).

carbon atoms of the thiazole (Th) heterocycle. Finally, a peak at 173 ppm is assigned to the carbonyl carbon atom of the carboxyl group.

After coupling MPT–Ph to the silica mesopores (Figure 2c), the resonances of the α, β and γ carbon atoms of the APTES linker at 10 ppm, 22 ppm and 42 ppm are still observed, which suggests that the linker is still attached to the surface. The signal at 62 ppm can be assigned to the methoxy carbon atom of the MPT–Ph dye. The resonances between 120 ppm and 149 ppm of the aromatic carbon atoms of the phenyl (Ph) ring are preserved. The signals at 117 ppm and between 161 ppm and 170 ppm previously assigned to the carbon atoms of the thiazole heterocycle are also still obtained. Most importantly, the resonance at 170 ppm can be assigned to the carbon atom of the newly formed amide bond between the APTES-linker and the dye. The chemical shift change in the carbonyl carbon from 173 ppm to 170 ppm indicates the conversion of the carboxylic carbon to an amide carbon.

To investigate the binding situation between the surface-bound NH_2 group and the COOH group of the dye, DNP-enhanced ^{15}N solid-state NMR was applied, which can detect the ^{15}N nuclei of an amide bond in natural abundance and avoids costly ^{15}N isotope labeling.[22]

The DNP-enhanced ^{15}N CP MAS NMR spectrum of the MPT–Ph dye-functionalized SBA-15 species (Figure 3a) shows a signal at −6 ppm. This signal is assigned either to the protonated (NH_3^+) or nonprotonated (NH_2) form of the nitrogen atom of the APTES-linker. The presence of this signal indicates unreacted amine groups on the surface. In addition, a second signal at 81 ppm is observed, which is assigned to the nitrogen atom of the amide group between the APTES-linker and the surface coupled dye. This clearly demonstrates the covalent binding of MPT–Ph to the mesoporous silica surface. Further-

more, the small signal at 165 ppm is characteristic of the pyridinium cation (Py^+–H). From the ^{15}N-chemical shift/pKa correlation data of heteroaromatic ring nitrogens in solid state complexes reported in a publication by *Lorente et al.*[23] and the pyridine ^{15}N chemical shift of pyridine in the solid state,[24] the high-field shift of 105 ± 10 ppm corresponds to a pKa of $0 \pm 1/2$. The residual signals at 251 ppm and 268 ppm can be assigned to the nonprotonated nitrogen atom of pyridine (Py) and the nitrogen atom of the thiazole heterocycle (Th).[15b]

To investigate the pH responsiveness, the dye was grafted to the surface of the mesoporous silica, and the pH value of the DNP matrix was adjusted to 1 by the addition of DCl. The pH change results in a color change from blue (pH 7) to green (pH 1) under UV light irradiation (352 nm). This color is maintained even after removing the excess liquid (Figure 3c), which proves the pH response of the surface-bound dye.

Additionally, a DNP-enhanced ^{15}N CP MAS NMR spectrum of the acidic sample was recorded to investigate the chemical changes in the dye induced by the pH change (Figure 3b). Comparing the spectrum recorded before (Figure 3a) and after pH adjustment, the signal at −11 ppm is preserved. At this pH, this signal is assigned to the protonated (NH_3^+) form of the nitrogen atom of the APTES-linker. The resonance of the amide nitrogen is still observed at 76 ppm, which clearly reveals the stability of the covalent MPT–Ph binding to the silica surface even at pH 1. Additionally, the signal of the protonated pyridine nitrogen (Py^+–H) is preserved at pH 1 and seems to be increased in intensity compared to that at pH 7.

In the region of higher chemical shift, only the signal at 238 ppm remains, which is assigned to the nitrogen atom of the thiazole heterocycle (Th). The signal of the nonprotonated nitrogen atom of pyridine (Py) is no longer observed. The pH switching mechanism of the dye suggests protonation of the
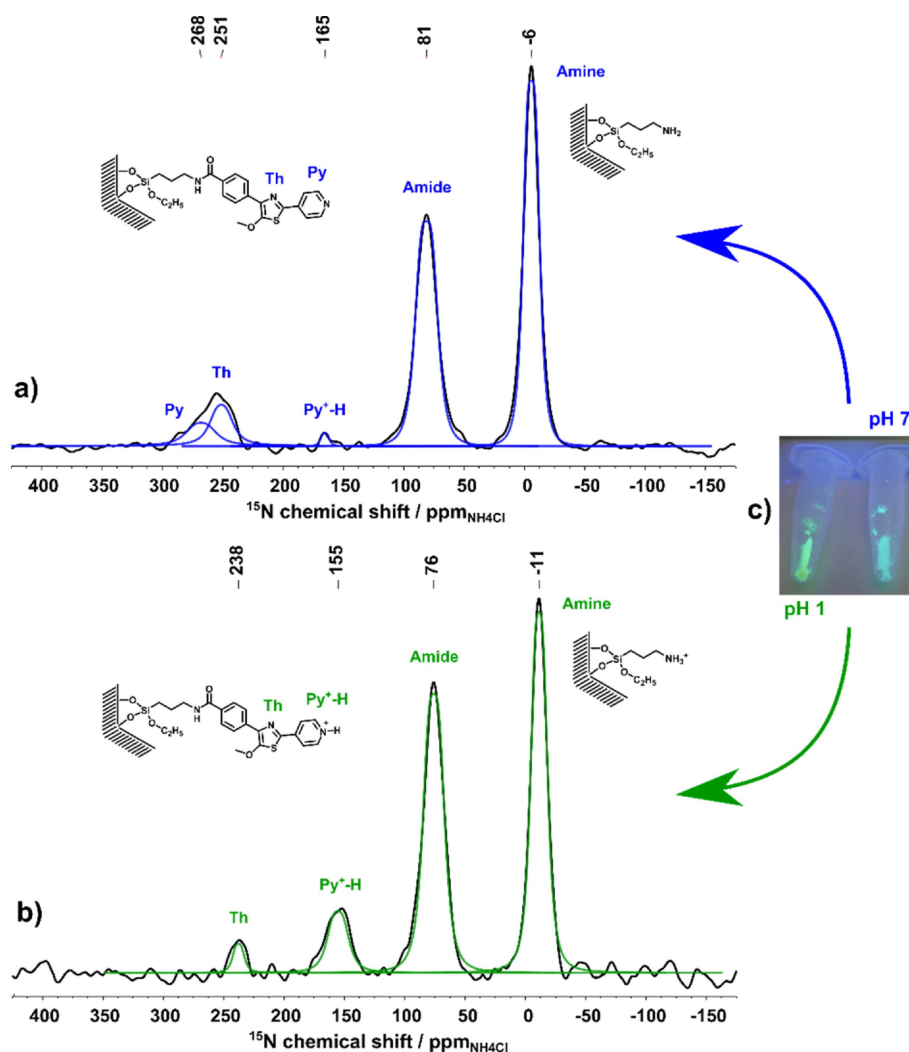
These are not the final page numbers! ⌐⌐

Figure 3. Comparison of DNP-enhanced ^{15}N CP MAS spectra of functionalized SBA-15 at a spinning rate of 8 kHz and at a nominal temperature of 110 K. Spectra of MPT—Ph dye-functionalized SBA-15 silica at pH 7 (a) and pH 1 (b). Comparison (c) of dried MPT—Ph dye-functionalized SBA-15 silica under UV light irradiation (352 nm) used for the NMR measurements.

pyridine nitrogen, which is in good agreement with this observation, since the signal intensity of the protonated pyridine nitrogen (Py$^+$—H) also increased.

Optical characterization of MPT—Ph functionalized silica thin films

From UV-vis measurements and determined by the *Lambert-Beer law* (Equation 1) where A is the measured Absorbance, d is twice the film thickness and the previously determined ε of $8070 \, mol \, l^{-1} \, cm^{-1}$, it is clear that the large pores (16 nm) can incorporate higher dye concentrations (c) ($0.24 \, mol \, l^{-1}$) than the 8 nm pores ($0.12 \, mol \, l^{-1}$) (Figure 4 a red line and purple line).

$$A = \varepsilon \cdot c \cdot d \qquad (1)$$

In accordance with Lambert-Beer's law, the amount of dye per substrate surface (c) and thus the maximum absorbance (A) can be adjusted by changing the mesoporous silica film thickness (d). Thus, the film thickness and pore size are critical parameters to adjust the total detectable dye amount, which is crucial for a visible coloration of the mesoporous silica film (Figure 4b). The UV-vis measurements confirm the homogeneous dye functionalization along the mesoporous silica film thickness, as the absorbance approximately doubles when the mesoporous thin films are twice as thick as the original (Figure 4a blue line vs purple line).

To investigate the infiltration of the measurement solution and diffusion into the mesoporous thin films at a relevant time scale for the experiments performed in this study, UV-vis measurements were performed directly after immersing the MPT—Ph functionalized and dry film into a test solution. The film was kept in the measurement solution for 60 minutes while measuring one UV-vis spectrum per minute. This test showed
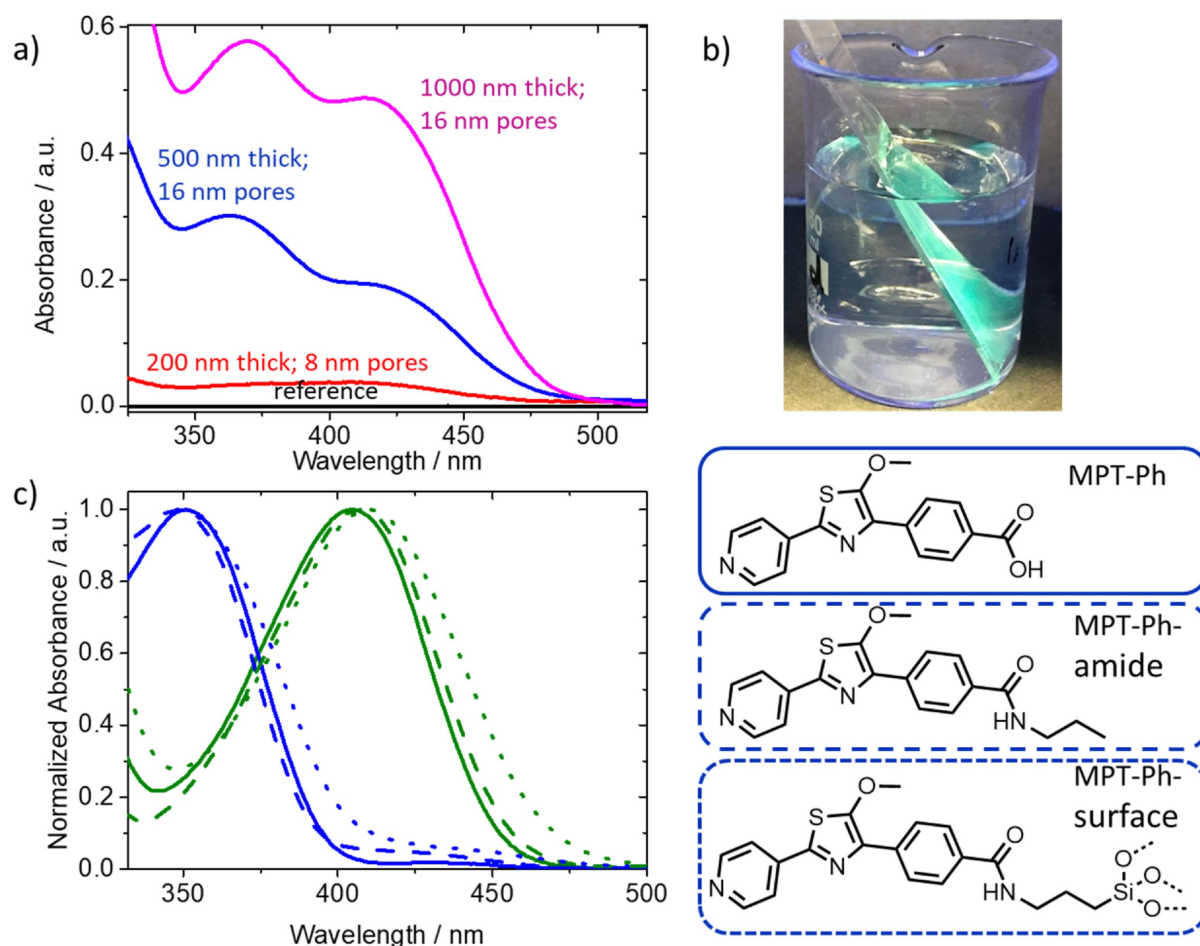
These are not the final page numbers! ↗↗

Figure 4. (a) UV-vis spectra of MPT–Ph functionalized mesoporous silica films with film thicknesses of 200 nm (red line), 500 nm (blue line) and 1000 nm (pink line). The black line is an unfunctionalized mesoporous silica film. Measurements were recorded at a solution pH of ~3; (b) Picture of an MPT–Ph functionalized mesoporous silica thin film under UV-light irradiation (365 nm); (c) UV-vis spectra and the corresponding chemical structures of MPT–Ph (solid lines), MPT–Ph-amide (dashed lines) and MPT–Ph-surface (dotted lines) of the protonated form at pH 1.5 (green) and the deprotonated form at pH 7.5 (blue).

no difference between the measurement at t = 0 minutes and t = 60 minutes (Figure S15), indicating that acid-base equilibrium of the incorporated MPT–Ph dye is obtained during sample preparation and that no dye leaching is observed. This also shows that the diffusion of solution through the film is not hindered and that the system can react quickly with a change in the solution pH. In addition, the UV-vis measurements show that the mesoporous silica film and the dye functionalization are stable towards the measurement solution for at least 60 minutes, while measurements are conducted in less than a minute.

To prove that the combination of MPT–Ph and mesoporous silica is suitable for pH investigation in thin mesoporous films, the pH responsiveness of the dye was confirmed after surface anchoring. As shown in Figure 4c, MPT–Ph-amide and the MPT–Ph-surface show the same pH responsive behavior as MPT–Ph. While MPT–Ph-amide (Figure 4c dashed lines) was used as a chemical analog to the surface-anchored MPT–Ph (Figure 4c solid lines), a slight influence of the surface is noticeable. The absorption maxima of the surface-anchored dye (Figure 4c dotted lines) are slightly redshifted compared to both dyes measured in bulk solution. It is not differentiated if this slight redshift originates from influences due to confinement or surface chemistry as the apparent pH in such nanoscale pores is always depending on both. The influence of confinement on photophysical dye characteristics is increasingly discussed especially for pores with diameters below 2 nm.[25] As the observed red-shift is minimal and the pH-response is still present we applied this grafted dye for apparent pH-detection.

Bulk vs confined pH measurements

For pH detection using MPT–Ph as a pH reporter, measurement solutions with a predetermined pH value between 8.4 and 1.7 were prepared. Their pH values were stabilized using PBS buffer solution (150 mM). Subsequently, UV-vis spectra were recorded. With decreasing pH, the absorption maximum at ~350 nm decreases, while the absorption maximum at 411 nm increases (Figure 5a). To determine the pKa value of MPT–Ph, the quotient of $\frac{[MPT-Ph-H^+]}{[MPT-Ph]}$ can be plotted against the measured
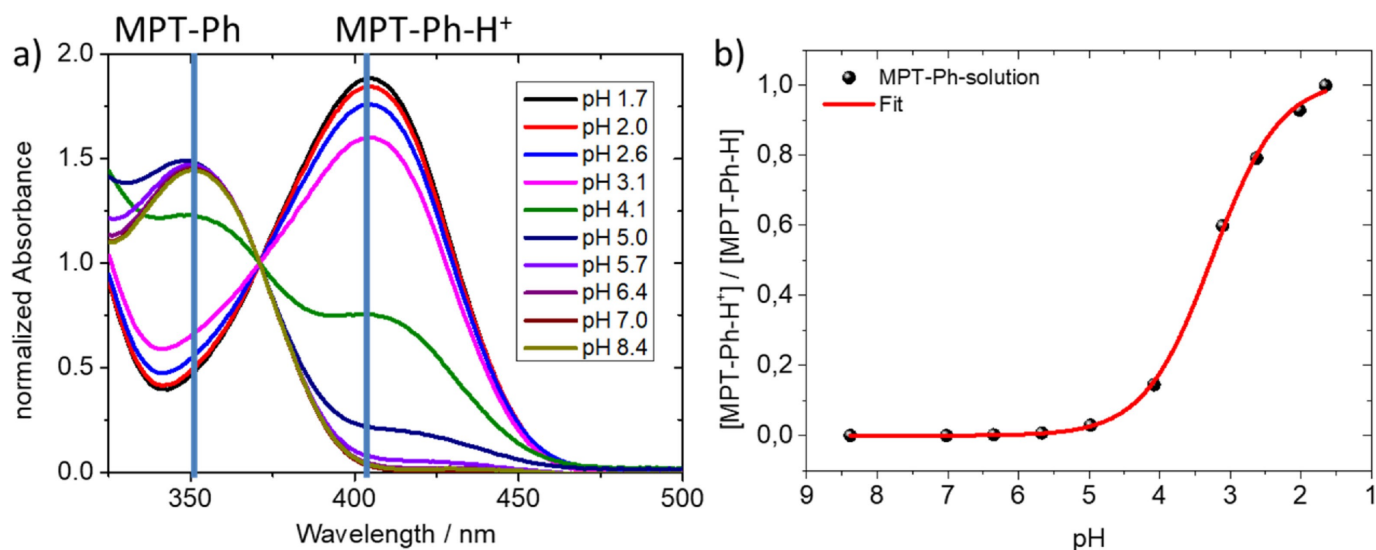
Figure 5. (a) UV-vis spectra of MPT—Ph at pH values between 8.4 and 1.7; (b) corresponding plot to measurements from (a), showing the quotient of MPT—Ph-H$^+$/MPT—Ph plotted against the solution pH value (black spheres). The red line shows a mathematical sigmoidal fit to determine the pKa value of MPT-Ph (pKa = 3.3).

solution pH value. A mathematical sigmoidal fit was used to determine the pKa value of 3.3 (Figure 4b).

The same procedure was further used to determine the pKa value of MPT—Ph-amide and that of the surface-bound MPT—Ph-surface derivative (Figure 6a). The results show that the difference between the residual carboxyl group of the MPT—Ph dye

(pKa 3.3) and the residual amide functional group in the MPT—Ph-amide dye (pKa 3.5) towards the resulting pKa value is very small. On the other hand, when entrapped in the nano-confined silica mesopores, MPT—Ph-surface shows a pKa value of 2.1. This pKa shift of more than one pH unit compared to its pKa value in solution (Figure 6a) indicates a ten-fold more acidic
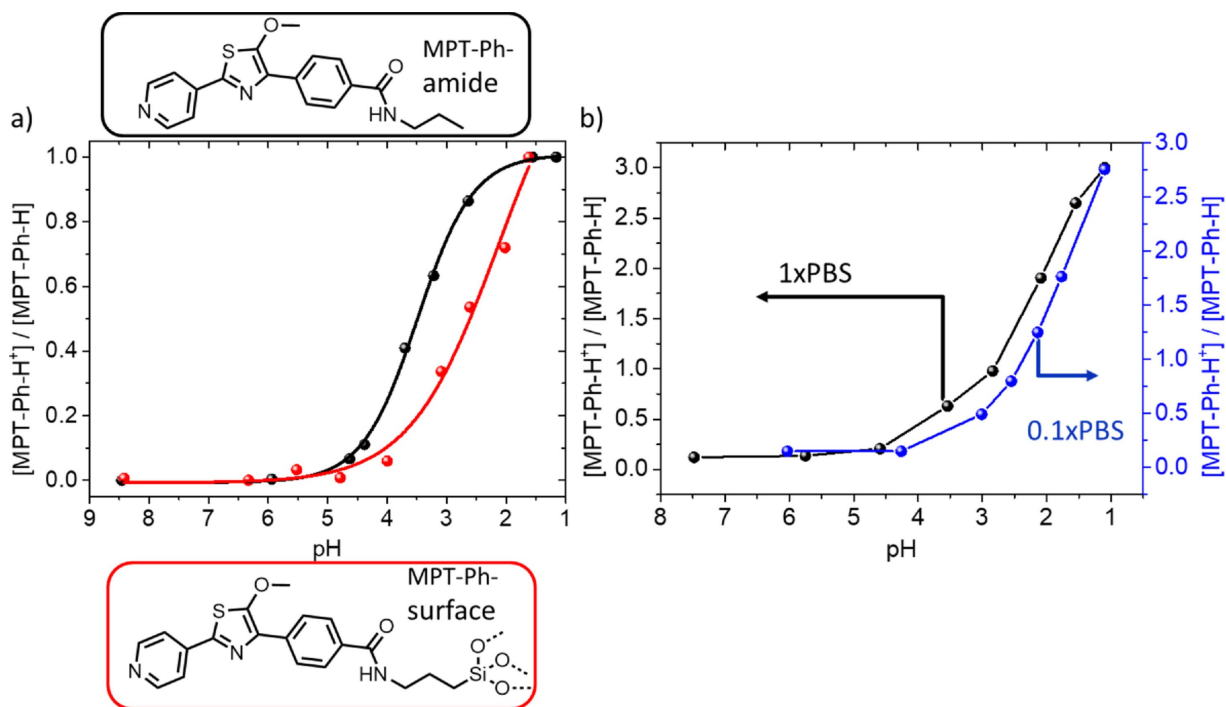

Figure 6. a) Quotient of MPT—Ph-amide-H$^+$/MPT—Ph-amide (black spheres) and MPT—Ph-surface-H$^+$/MPT—Ph-surface (red spheres) plotted against the solution pH value. Black and red lines show the corresponding mathematical sigmoidal fit to determine the pKa value of MPT—Ph-amide (pKa = 3.5) and MPT—Ph-surface (pKa = 2.1). b) Quotient of MPT-Ph-surface-H+/MPT-Ph-surface plotted against the solution pH value at different ionic strengths of 150 mM (black line) and 15 mM (blue line)

These are not the final page numbers! ⌐⌐

environment in mesopores than the measurements in bulk solution. The observed confinement effects detected as equilibrium shift which result in the apparent pH of course relate to changes in surface chemistry as well as the influence of spatial confinement. Both aspects are not separated in this study.

These findings using MPT–Ph as a new pH-reporter dye molecule sensitive to the required pH region (pH 1–5) in which mesoporous silica responds are in accordance with previous findings from our group investigating the pKa value of short oligomer chains in silica mesopores as well as with theoretical simulations for short polymer chains in ion channels.[9a,11a]

Additionally, titration experiments with the surface-attached MPT–Ph derivate were carried out at ionic strengths of 150 and 15 mM PBS buffer. The obtained results clearly show that at a lower salt concentration of 0.1xPBS (15 mM) compared to 1xPBS (150 mM) and thus an increased Debye-screening length from approximately 0.7 nm to 2.5 nm, the protonation process is even further shifted towards more extreme (here acidic) conditions (Figure 6b and Figure S16).

Conclusion

A new thiazol-based ratiometric pH reporting dye, compatible with the pKa value of mesoporous silica, has been synthesized and fully characterized regarding its optical properties. This MPT–Ph dye covers a completely different sensitivity range with an acidic pKa value of 3.5 compared to other established dyes for ratiometric pH detection, such as SNARF. As demonstrated in this study, this more acidic pH range is especially interesting to follow confinement effects in nanoscale pores on pH, such as in mesoporous silica, in which the pH value plays a crucial role for various applications from separation processes to drug delivery. MPT–Ph can be easily grafted to the silica surface and mesopore wall. This study proves the covalent bond between the dye and surface by solid-state NMR studies. Advanced solid-state NMR DNP methods further prove the protonation of the nitrogen atom of the MPT–Ph molecule at acidic pH within silica mesopores.

The developed ratiometric MPT–Ph dye has been successfully employed to measure pH variations between bulk solutions and nanoscale silica pores and enabled in situ readout of the "pH value" in silica mesopores by simple UV-vis measurements. The obtained results indicate a background electrolyte-dependent pKa shift of at least one pH unit under nanoconfined conditions compared to the pKa in bulk solution. To the best of our knowledge, this study is the first to employ a direct measurement approach using a covalently coupled reporter molecule to determine the pH value inside of silica mesopores and to compare it with data from the bulk solution to determine the confinement effect on the pH value in silica mesopores. The obtained results are in good agreement with previous experimental findings using indirect measurements and theoretical simulations.

Experimental Section

Preparation of 1x PBS buffer solution: In 1000 ml distilled water, 8.00 g (136.9 mmol) NaCl, 0.20 g (2.7 mmol) KCl, 1.42 g Na_2HPO_4 (10.0 mmol) and 0.27 g (2.0 mmol) KH_2PO_4 were dissolved, and the solution was stirred for 24 hours before being used for UV-vis measurements.

Preparation of Mesoporous Silica Thin Films: Mesoporous silica films were prepared via sol-gel chemistry using tetraethoxysilane (TEOS) as an inorganic precursor. The sol contained an amphiphilic triblock copolymer, Pluronic® F127 (BioReagent, Sigma-Aldrich, 13,800 g mol^{-1}), in different ratios, which undergoes micellization upon solvent evaporation, resulting in the formation of a porous inorganic network. A typical synthesis of films with 8 nm (or 16 nm) pores used 1.37 g (2.61 g) of Pluronic® F127, which was dissolved in 33.8 ml (24.0 ml) of absolute ethanol and 5.22 ml of H2O, and 0.33 ml of 37% HCl (6.4 ml of 0.05 M HCl). Then, 6.55 mL (4.88 ml) of TEOS was added to the mixture, and the solution was stirred overnight under ambient conditions before being used to prepare films through evaporation-induced self-assembly (EISA). Dip-coating was performed in a climate-controlled chamber at a temperature of 23 °C and a relative humidity of 50%, at a withdrawal speed of 2 mm s^{-1}. After aging the films for 1 h at 50% relative humidity and at 23 °C, they were subjected to the following thermal treatment: two 1-h steps at 60 and 130 °C followed by heating to 350 °C with a heating rate of 1 °C/min. Finally, the films were stabilized at 350 °C for 2 h before cooling to room temperature.

Preparation of amino-functionalized SBA-15: Based on our protocol reported earlier[21] in a typical procedure, 7.10 g (0.017 eq) Pluronic P123 was dissolved in 191.2 ml (165.0 eq) of deionized water, and 36.0 ml (6.0 eq) of 37 wt% HCl was added, which resulted in a HCl concentration of 1.9 mol/L. The solution was heated to 40 °C, and 12.0 g (0.8 eq) of tetraethyl orthosilicate (TEOS) was added slowly while stirring. Stirring was continued for 1 h, and a white precipitate was formed. After this prehydrolysis step, 3.19 g (0.2 eq) of (3-aminopropyl)triethoxysilane (APTES) was added. The suspension was stirred for 24 h at 40 °C and then transferred into a polypropylene (PP) bottle. The bottle was stored under static conditions at 100 °C for 48 h. The white precipitate was filtered off and washed two times with deionized water, ethanol and acetone. The product was dried in an oven at 90 °C overnight. The remaining template was removed by Soxhlet extraction with ethanol for 48 h. The product was dried under high vacuum, yielding 3.19 g of functionalized SBA-15.

Synthesis of MPT–Ph: A total of 489 mg of MPT–Br, 401 mg of 4-carboxyphenylboronic acid and 518 mg of K_2CO_3 were dissolved in a mixture of 40 ml dioxan and 10 ml H_2O, and this mixture was deoxygenated for 15 minutes by nitrogen bubbling. Then, the X-Phos Pd–G2 precatalyst was added (90 mg), and the reaction mixture was heated to 80 °C for 16 h. MPT–Ph was isolated by column chromatography using methanol and ethyl acetate as the eluent. The yield was 400 mg (71%). ^{1}H NMR (700 MHz, DMSO-d6) δ 8.67 (d, J = 5.7 Hz, 2H), 8.25 (d, J = 6.0 Hz, 2H), 7.96 (d, J = 8.2 Hz, 2H), 7.81 (d, J = 8.2 Hz, 2H), 4.06 (s, 3H); HRMS (ESI) *m/z*: [M + H]$^+$ calcd for $C_{16}H_{12}N_2O_3S$, 313.06; found, 313.07.

Synthesis of MPT–Ph-amide: Fifty milligrams of MPT–Ph was dissolved in 15 ml dimethyl formamide (DMF). Subsequently, 45 μl diisoprpylethylamine (DIPEA) and 61 mg HATU were added, and the solution was stirred for 15 minutes. Then, 5.7 mg propylamine was added, and the reaction mixture was stirred for 24 h at room temperature. MPT–Ph-amide was isolated by column chromatography using methanol and ethyl acetate as the eluent as well as HPLC. The yield was 40 mg (71%). ^{1}H NMR (700 MHz, methanol-d4) δ 8.78–8.75 (m, 2H), 8.38–8.35 (m, 2H), 8.22–8.18 (m, 2H), 7.92–7.88

These are not the final page numbers! ⬈⬈

(m, 2H), 4.29 (s, 3H), 3.37 (t, J = 7.2 Hz, 2H), 1.67 (h, J = 7.4 Hz, 2H), 1.00 (t, J = 7.4 Hz, 3H); 13 C NMR (176 MHz, MeOD) δ 169.48, 165.90, 148.77, 146.06, 144.55, 137.66, 136.80, 134.49, 128.24, 127.63, 122.16, 65.46, 49.26, 49.10, 48.97, 48.85, 48.73, 48.61, 48.49, 48.37, 42.56, 23.49, 11.51; HRMS (ESI) *m/z*: $[M+H]^+$ calcd for $C_{19}H_{19}N_3O_3S$, 354.13; found, 354.13.

Aminopropyltrimethoxysilane (APTMS) grafting on mesoporous silica thin films: A 0.05 wt% solution of APTMS in dry toluene (51.1 µl in 140 ml of dry toluene) was prepared and used to overlay the glass substrates in a Schlenk flask. Afterwards, the samples in the Schlenk flasks were kept at room temperature overnight. Then, the samples were rinsed and extracted with ethanol.

Coupling of MPT–Ph to amino-functionalized mesoporous silica films: Under Schlenk conditions, 10 mg of MPT–Ph was dissolved in dry dimethyl formamide (DMF). Subsequently, 10.9 µl diisoprpylethyl-amine (DIPEA) and 24.3 mg HATU were added, and the solution was stirred for 15 minutes. Then, the amino-functionalized meso-porous silica film was immersed in the solution for 24 h. Afterwards, the film was rinsed with DMF and methanol before being dried.

Coupling of MPT–Ph to amino-functionalized mesoporous silica (SBA-15): MPT–Ph was coupled by activating its COOH group with 1-[bis (dimethylamino)methylene]-1H-1,2,3-triazolo[4,5-b]pyridinium 3-oxide hexafluorophosphate (HATU) and N-ethyl-N-(propan-2-yl) propan-2-amine (DIEA). A total of 121 mg (1.0 eq) of *MPT–Ph* and 145 mg (0.98 eq) of HATU were dissolved in 8 ml of dry DMF. The solution was activated by adding 100 mg (2.0 eq) of DIEA and shaking for 2 min. Then, 400 mg of dried amino-functionalized SBA-15 was added to the activated amino acid solution. The suspension was shaken at 1000 rpm at RT for 16 h. The solid was filtered off and washed two times with DMF, distilled water and acetone. The functionalized SBA-15 was dried under reduced pressure at room temperature, which resulted in 475 mg of colorless solid.

NMR measurements: ^{1}H-, ^{13}C-, and 2D-NMR experiments were conducted on a Bruker AV-III 600 or Bruker AV-III HD 700 NMR spectrometer. To shift the water signal and to protonate, MPT–Ph and MPT–Ph-amide DCl (37%) were added to some samples.

Solid-state NMR measurements: [13]CP-MAS and ^{29}Si CP-MAS solid-state NMR measurements were carried out at room temperature on a Bruker AVANCE II+400 spectrometer corresponding to a frequency of 400.13 MHz for ^{1}H, 100.62 MHz for ^{13}C, and 79.48 MHz for [29]Si employing a Bruker 4 mm double resonance probe. Spectra were recorded with a contact time of 1.5 ms for ^{13}C and 6.5 ms for [29]Si with a recycle delay of 2 s. Protons were decoupled during data acquisition with the tppm15 decoupling sequence.[26] Referencing was performed with respect to tetramethylsilane (TMS) (0 ppm) employing adamantane (−38.5 ppm) and kaolin (−92.5 ppm) as external standards for ^{13}C and [29]Si, respectively.

Dynamic nuclear polarization (DNP)-enhanced NMR measurements: Samples for DNP experiments were prepared by impregnating approximately 15 mg of the sample with 15 µl of a 15 mM AMUPol in glycerol-d_8/D_2O/H_2O (60:30:10 v/v/v) solution. Samples were packed into 3.2 mm sapphire rotors and sealed with a Teflon plug and a ZrO_2 driving cap. For pH adjustment of the matrix, 38% DCl was used.

All DNP experiments were performed on a Bruker Avance III 400 DNP spectrometer equipped with an Ascend 400 DNP magnet system and a low-temperature ^{1}H/X/Y probe. DNP-enhanced spectra were measured with microwave irradiation (MW on). All DNP-enhanced spectra were recorded at a field of 9.4 T corresponding to frequencies of 400.25 MHz for ^{1}H, 100.58 MHz for ^{13}C and 40.53 MHz for ^{15}N at a nominal temperature of 110 K and at a spinning rate of 8 kHz. The recycle delay was taken as 1.3 T_1 (^{1}H)

according to the literature,[27] where T_1 (^{1}H) is the build-up time for ^{1}H obtained from a saturation recovery experiment recorded with microwave irradiation. During data acquisition, tppm20[21] hetero-nuclear decoupling was applied to the ^{15}N CP MAS spectra. The ^{15}N CP MAS spectra were recorded with contact times of 6 ms and referenced with NH_4Cl as an external standard (chemical shift of 0 ppm).

UV-vis measurements: UV-vis measurements were performed using an Agilent Cary 60 UV-vis spectrophotometer or an AnalytikJena Specord S600 spectrophotometer using PMMA cuvettes. The concentrations of sample solutions were kept below 50 mM, and the dye-functionalized mesoporous silica films were fixed straight in the cuvette diagonal to the light beam.

Fluorescence measurements: The steady-state (time-integrated) fluorescence spectra were recorded with a Jasco FP-8500 spectro-fluorometer in 4×10 mm UV-grade quartz cuvettes. The spectra were corrected for the offset, device detection sensitivity, wave-length-dependent excitation light intensity and reabsorption con-tributions. For the determination of the fluorescence quantum yields, the FP-8500 spectrofluorometer was equipped with a 100 mm integrating sphere from Jasco (ILF-835), and the calcu-lations were carried out with Origin 2019 data analysis software.

The time-correlated single photon counting (TCSPC) measurements were performed with a self-assembled setup with a PicoQuant photomultiplier tube (PMT) PMA–C 182-M for single photodetec-tion. Data were acquired with a TimeHarp 260 PICO single PCIe card, and data analysis and multiexponential fitting were executed with FluoFit Pro 4.6 software from PicoQuant. The samples were also prepared in 4x10 mm quartz glass cuvettes, and the excitation of the samples was carried out with pulsed light-emitting diodes (LEDs), enabling a maximum time resolution of approximately 200 ps. The instrumental response function (IRF) was recorded with a TiO2 suspension as a scattering sample. For the detection of the sample fluorescence decay curves, colored glass filters (Schott AG) were used to suppress stray light.

Supporting Information

Supporting information is available from the Wiley Online Library or from the author.

Acknowledgments

[1] C. T. Kresge, M. E. Leonowicz, W. J. Roth, J. C. Vartuli, J. S. Beck, *Nature* **1992**, *359*, 710–712.

[2] a) T. Nasir, G. Herzog, M. Hebrant, C. Despas, L. Liu, A. Walcarius, *ACS Sens.* **2018**, *3*, 484–493; b) A. Walcarius, E. Sibottier, M. Etienne, J. Ghanbaja, *Nat. Mater.* **2007**, *6*, 602–608; c) K. Wang, J. He, *ACS Appl. Mater. Interfaces* **2018**, *10*, 11189–11196.

[3] a) Z. Alothman, *Materials* **2012**, *5*, 2874–2902; b) M. Kruk, *Isr. J. Chem.* **2012**, *52*, 246–255.

[4] F. H. van der Heyden, D. J. Bonthuis, D. Stein, C. Meyer, C. Dekker, *Nano Lett.* **2006**, *6*, 2232–2237.

[5] F. Hoffmann, M. Cornelius, J. Morell, M. Froba, *Angew. Chem. Int. Ed. Engl.* **2006**, *45*, 3216–3251.

[6] R. Narayan, U. Y. Nayak, A. M. Raichur, S. Garg, *Pharmaceutics* **2018**, *10*, 118–166.

[7] M. Tagliazucchi, O. Azzaroni, I. Szleifer, *J. Am. Chem. Soc.* **2010**, *132*, 12404–12411.

[8] a) A. Brunsen, J. Cui, M. Ceolin, A. del Campo, G. J. Soler-Illia, O. Azzaroni, *Chem. Commun. (Camb.)* **2012**, *48*, 1422–1424; b) K. Huang, I. Szleifer, *J. Am. Chem. Soc.* **2017**, *139*, 6422–6430; c) X. Hou, W. Guo, L. Jiang, *Chem. Soc. Rev.* **2011**, *40*, 2385–2401; d) X. Huang, D. Appelhans, P. Formanek, F. Simon, B. Voit, *ACS Nano* **2012**, *6*, 9718–9726; e) G. Perez-Mitta, A. G. Albesa, W. Knoll, C. Trautmann, M. E. Toimil-Molares, O. Azzaroni, *Nanoscale* **2015**, *7*, 15594–15598; f) G. V. R. R. Qiang Fu, L. K. Ista, Y. Wu, B. P. Andrzejewski, L. A. Sklar, T. L. Ward, G. P. Lopez, *Adv. Mater.* **2003**, *15*, 1262–1266; g) J. Wen, K. Yang, F. Liu, H. Li, Y. Xu, S. Sun, *Chem. Soc. Rev.* **2017**, *46*, 6024–6045; h) F. Yu, X. Tang, M. Pei, *Microporous Mesoporous Mater.* **2013**, *173*, 64–69.

[9] a) R. Brilmayer, S. Kübelbeck, A. Khalil, M. Brodrecht, U. Kunz, H. J. Kleebe, G. Buntkowsky, G. Baier, A. Andrieu-Brunsen, *Adv. Mater. Interfaces* **2020**, *7*; b) M. H. Sun, S. Z. Huang, L. H. Chen, Y. Li, X. Y. Yang, Z. Y. Yuan, B. L. Su, *Chem. Soc. Rev.* **2016**, *45*, 3479–3563.

[10] S. E. Kim, L. Zhang, K. Ma, M. Riegman, F. Chen, I. Ingold, M. Conrad, M. Z. Turker, M. Gao, X. Jiang, S. Monette, M. Pauliah, M. Gonen, P. Zanzonico, T. Quinn, U. Wiesner, M. S. Bradbury, M. Overholtzer, *Nat. Nanotechnol.* **2016**, *11*, 977–985.

[11] a) F. M. Gilles, M. Tagliazucchi, O. Azzaroni, I. Szleifer, *J. Phys. Chem. C* **2016**, *120*, 4789–4798; b) M. Stanzel, R. Brilmayer, M. Langhans, T. Meckel, A. Andrieu-Brunsen, *Microporous Mesoporous Mater.* **2019**, *282*, 29–37; c) A. Yamaguchi, M. Namekawa, T. Kamijo, T. Itoh, N. Teramae, *Anal. Chem.* **2011**, *83*, 2939–2946; d) P. Gong, T. Wu, J. Genzer, I. Szleifer, *Macromolecules* **2007**, *40*, 8765–8773; e) O. Schepelina, I. Zharov, *Langmuir* **2008**, *24*, 14188–14194.

[12] a) C. Richter, C. Schneider, M. T. Quick, P. Volz, R. Mahrwald, J. Hughes, B. Dick, U. Alexiev, N. P. Ernsting, *Phys. Chem. Chem. Phys.* **2015**, *17*, 30590–30597; b) C. Thörn, N. Carlsson, H. Gustafsson, K. Holmberg, B. Åkerman, L. Olsson, *Microporous Mesoporous Mater.* **2013**, *165*, 240–246;

c) M. Sulpizi, M. P. Gaigeot, M. Sprik, *J. Chem. Theory Comput.* **2012**, *8*, 1037–1047; d) J. M. Rosenholm, T. Czuryszkiewicz, F. Kleitz, J. B. Rosenholm, M. Lindén, *Langmuir* **2007**, *23*, 4315–4323.

[13] a) J. Lei, L. Wang, J. Zhang, *Chem. Commun. (Camb.)* **2010**, *46*, 8445–8447; b) M.-H. Zheng, J.-Y. Jin, W. Sun, C.-H. Yan, *New J. Chem.* **2006**, *30*, 1192.

[14] a) S. Brasselet, W. E. Moerner, *Single Mol.* **2000**, *1*, 17–23; b) S. Wan, Y. Zheng, J. Shen, W. Yang, M. Yin, *ACS Appl. Mater. Interfaces* **2014**, *6*, 19515–19519; c) R. Martínez-Máñez, F. Sancenón, M. Biyikal, M. Hecht, K. Rurack, *J. Mater. Chem.* **2011**, *21*; d) J. Han, A. Loudet, R. Barhoumi, R. C. Burghardt, K. Burgess, *J. Am. Chem. Soc.* **2009**, *131*, 1642–1643; e) H. L. Lee, S. J. Lord, S. Iwanaga, K. Zhan, H. Xie, J. C. Williams, H. Wang, G. R. Bowman, E. D. Goley, L. Shapiro, R. J. Twieg, J. Rao, W. E. Moerner, *J. Am. Chem. Soc.* **2010**, *132*, 15099–15101; f) J. Ji, N. Rosenzweig, C. Griffin, Z. Rosenzweig, *Anal. Chem.* **2000**, *72*, 3497–3503.

[15] a) L.-L. Li, H. Sun, C.-J. Fang, J. Xu, J.-Y. Jin, C.-H. Yan, *J. Mater. Chem.* **2007**, *17*, 4492; b) I. G. Shenderovich, G. Buntkowsky, A. Schreiber, E. Gedat, S. Sharif, J. Albrecht, N. S. Golubev, G. H. Findenegg, H.-H. Limbach, *J. Phys. Chem. B* **2003**, *107*, 11924–11939.

[16] a) S. Charier, O. Ruel, J. B. Baudin, D. Alcor, J. F. Allemand, A. Meglio, L. Jullien, *Angew. Chem. Int. Ed. Engl.* **2004**, *43*, 4785–4788; b) M. H. Zheng, M. M. Zhang, H. H. Li, J. Y. Jin, *J. Fluoresc.* **2012**, *22*, 1421–1424.

[17] K. Yamaguchi, T. Murai, Y. Tsuchiya, Y. Miwa, S. Kutsumizu, T. Sasamori, N. Tokitoh, *RSC Adv.* **2017**, *7*, 18132–18135.

[18] a) M. Y. Yang, X. L. Zhao, M. H. Zheng, Y. Wang, J. Y. Jin, *J. Fluoresc.* **2016**, *26*, 1653–1657; b) Y. Watanabe, W. Sungnoi, A. O. Sartorio, M. Zeller, A. Wei, *Mater. Chem. Front.* **2020**, *4*, 899–904.

[19] a) E. W. Driscoll, J. R. Hunt, J. M. Dawlaty, *J. Phys. Chem. A* **2017**, *121*, 7099–7107; b) A. Brenlla, M. Veiga, J. L. Perez Lustres, M. C. Rios Rodriguez, F. Rodriguez-Prieto, M. Mosquera, *J. Phys. Chem. B* **2013**, *117*, 884–896.

[20] N. Herzog, R. Brilmayer, M. Stanzel, A. Kalyta, D. Spiehl, E. Dörsam, C. Hess, A. Andrieu-Brunsen, *RSC Adv.* **2019**, *9*, 23570–23578.

[21] M. Brodrecht, H. Breitzke, T. Gutmann, G. Buntkowsky, *Chemistry* **2018**, *24*, 17814–17822.

[22] a) M. Brodrecht, B. Kumari, A. Thankamony, H. Breitzke, T. Gutmann, G. Buntkowsky, *Chemistry* **2019**, *25*, 5214–5221; b) M. Werner, A. Heil, N. Rothermel, H. Breitzke, P. B. Groszewicz, A. S. Thankamony, T. Gutmann, G. Buntkowsky, *Solid State Nucl. Magn. Reson.* **2015**, *72*, 73–78.

[23] P. Lorente, I. G. Shenderovich, N. S. Golubev, G. S. Denisov, G. Buntkowsky, H.-H. Limbach, *Magn. Reson. Chem.* **2001**, *39*, S18-S29.

[24] E. Gedat, A. Schreiber, G. H. Findenegg, I. Shenderovich, H. H. Limbach, G. Buntkowsky, *Magn. Reson. Chem.* **2001**, *39*, S149–S157.

[25] a) E. A. Dolgopolova, A. A. Berseneva, M. S. Faillace, O. A. Ejegbavwo, G. A. Leith, S. W. Choi, H. N. Gregory, A. M. Rice, M. D. Smith, M. Chruszcz, S. Garashchuk, K. Mythreye, N. B. Shustova, *J. Am. Chem. Soc.* **2020**, *142*, 4769–4783; b) A. Baldridge, S. R. Samanta, N. Jayaraj, V. Ramamurthy, L. M. Tolbert, *J. Am. Chem. Soc.* **2011**, *133*, 712–715; c) A. Ghodbane, W. Brett Fellows, J. R. Bright, D. Ghosh, N. Saffon, L. M. Tolbert, S. Fery-Forgues, K. M. Solntsev, *J. Mater. Chem. C* **2016**, *4*, 2793–2801; d) I. H. Choi, S. Bin Yoon, S. Huh, S. J. Kim, Y. Kim, *Sci. Rep.* **2018**, *8*, 9838.

[26] I. Scholz, P. Hodgkinson, B. H. Meier, M. Ernst, *J. Chem. Phys.* **2009**, *130*, 114510.

[27] S. Lange, A. H. Linden, U. Akbey, W. T. Franks, N. M. Loening, B. J. van Rossum, H. Oschkinat, *J. Magn. Reson.* **2012**, *216*, 209–212.

FULL PAPER

A new ratiometric thiazol-based dye (MPT—Ph) for pH detection in silica mesopores is presented, and its properties are characterized by optical spectroscopy, solid-state NMR and DNP-enhanced solid-state NMR. Direct in situ measurements of the local apparent pH value in silica mesopores by a simple UV-vis spectroscopy method are presented. The results enable direct measurements of nanoconfinement-induced pKa shifts and prove the apparent pH shifts of at least one pH unit.
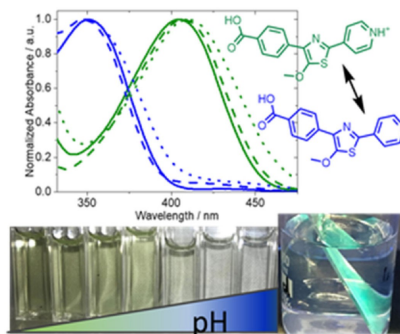
Dr. R. Brilmayer, Dr. M. Brodrecht, C. Kaiser, Dr. H. Breitzke, Dr. B. Kumari, Prof. Dr. J. Wachtveitl, Prof. Dr. G. Buntkowsky, Prof. Dr. A. Andrieu-Brunsen**

1 – 12

The Interplay of Nanoconfinement and pH from the Perspective of a Dye-Reporter Molecule